Draft version June 21, 2024
Typeset using LaTeX **twocolumn** style in AASTeX631

TESS Subgiant Asteroseismology in the Continuous Viewing Zones

Sophia Grusnis[1] and Jamie Tayar[1]

[1] *University of Florida*
Gainesville, FL 32611, USA

ABSTRACT

Asteroseismology, the study of stellar oscillations, and stellar modeling both offer profound insights into the fundamental properties and evolution of stars. With `pySYD`, a new open-source Python package, we were able to constrain the asteroseismic global parameters, ν_{max} and $\Delta\nu$, for 82 solar-oscillating subgiant and lower giant stars, filling in the region between the *Kepler* dwarfs and giants. Using asteroseismic scaling relations, we were able to compute seismic masses, radii, and surface gravities for our entire sample with average errors of 0.15 $M_{\odot}$, 0.23 $R_{\odot}$, and 0.059 dex respectively. Using 4 stellar modeling grids we determine and compare stellar ages for our sample. We find that our age distribution from stellar modeling is consistent with other local star samples. We find small consistent offsets from model predictions across our regime, but offsets were worse at higher gravities ($\log(g) \geq 3.5$), suggesting the need for better calibration. Finally, we discuss our sample in the context of galactic archaeology and show how ages like these could be used to identify and study binary and galactic evolution in the future. All in all, we show that asteroseismology can be successfully performed with *TESS* data and can continue to make an impact on our understanding of stellar physics and galactic archaeology.

1. INTRODUCTION

Our proficiency in stellar modeling is key to understanding many facets in astronomy. However, stellar models are based on many free parameters which need calibration and experimentation. In order to check, calibrate, and improve the models, we need a sample of stars with known mass, radius, temperature, and composition. Previous efforts have used eclipsing binaries (Higl & Weiss 2017) or stars in open clusters (Kalirai & Richer 2010; Fritzewski et al. 2024), but asteroseismology allows us to do similar work for the more numerous single stars.

Asteroseismology, the study of stellar oscillations, provides precise and accurate stellar parameters which we use to check these models (Quirion et al. 2010; Rodrigues et al. 2017; Rendle et al. 2019). To test these models, we have asteroseismically characterized some of the best subgiant solar-like oscillators in the *TESS* (Ricker et al. 2015) Continuous Viewing Zones (CVZs) at both the North Ecliptic Pole and South Ecliptic Pole. Solar-like oscillators are defined as stars whose pressure-mode oscillations are excited by convection, like our Sun (Aerts et al. 2010). These types of oscillators include dwarfs cooler than about 6300 K, subgiant stars, and giant branch stars. For solar-like oscillators, each star displays a characteristic pattern of oscillations with a Gaussian envelope around the frequency at maximum power, ν_{max}, with a regular frequency separation, $\Delta\nu$. These global parameters are used to find seismic masses and radii using a scaling off of the solar values (Kjeldsen & Bedding 1995).

The *Kepler* (Gilliland et al. 2010) and *TESS* (Ricker et al. 2015) satellites have measured precise light curves of hundreds of thousands of stars. Significant work has been done using the *Kepler* data to test our understanding of giants and dwarfs (Bedding et al. 2010; Gilliland 2011; Sreenivas et al. 2024). However, the subgiant and lower giant stars were understudied in *Kepler*. For subgiant stars, oscillations tend to occur at frequencies around 200-400 μHz and therefore require high precision at a cadence faster than 30 minutes. During the *Kepler* mission, the high cadence slots were generally used for dwarf and main sequence (MS) turnoff stars, so only a handful of subgiant and lower giant stars were included in (Deheuvels et al. 2012, 2014; Li et al. 2020b).

These stars are particularly interesting because on the subgiant branch, luminosity is strongly correlated with mass and age, allowing a possible avenue for the estimation of large numbers of precise ages (Xiang et al. 2017;

Corresponding author: Sophia Grusnis
sophiagrusnis@gmail.com

Li et al. 2020a; Xiang & Rix 2022). However this is also a region where models can differ significantly (do Nascimento et al. 2012; Hon et al. 2020). Therefore, using this technique requires careful calibration of the models to ensure they represent a correct mapping between luminosity and age.

Since these stars were understudied in *Kepler*, we turn to *TESS* as a possible avenue for this calibration, and in particular to a set of stars in the *TESS* CVZs, regions having an angle about 78° above and below the ecliptic plane, which were targeted for 2 minute cadence observation with more than 1 year of data for each subgiant star. We know from previous work like Schofield et al. (2019); Huber et al. (2019); Hatt et al. (2023) and Zhou et al. (2024) that this is enough data to do asteroseismology with our sample and compare our findings with the predictions of stellar models.

2. METHODS

2.1. *Sample Selection*

The stars in our sample were chosen for their potential for detailed seismic characterization in the region between dwarfs and giants that was understudied in *Kepler*. We wanted stars that have many months of data, which was most common in the *TESS* CVZs. We targeted stars that had the potential to be cool enough to have mixed modes detected (Mosser et al. 2014), i.e. an effective temperature less than or equal to 5600K, but were small enough that they would be unlikely to be well studied in the initial 30-minute cadence full frame images ($\log(g) \geq 3.3$). We used the Asteroseismic Target List (Schofield et al. 2019), and the detection probabilities therein to prioritize stars; in the South we required stars in our sample to have a detection probability greater than 50% from *Gaia* DR1 (Lindegren et al. 2016), in the North we required stars to have a detection probability greater than 50% using *Gaia* DR2 (Lindegren et al. 2018). We also prioritized stars that already had high resolution spectroscopic data at the time of targeting.

2.2. *Light Curve Creation*

To measure oscillations we require a star's light curve and power spectrum. Given the *TESS* observing strategy and our focus on the CVZs, most of our stars have about 24 months of data with a gap of at least 1 year in between the observed sectors. To collect these light curves, we made use of `Lightkurve`, a Python package for *Kepler* and *TESS* data analysis (Lightkurve Collaboration et al. 2018). Before any corrections, we used `Lightkurve` (v 2.4.2) to download all the available sectors to look for odd variations and large time gaps (Figure 1a). We excluded sectors 17 and 50 from our analysis because of the extra noise for many stars, as well as large gaps in the *TESS* data, which are times 2458764.6-2458789.7, 2458982.2-2459420.0, 2459446.5-2459579.8, and 2459664.3-2459693.0 BTJD days. We chose to remove the big gaps in the *TESS* data collection because we found these gaps would alter our inferred seismic results (García et al. 2014; Bedding & Kjeldsen 2022). We then used `Lightkurve` to smooth and normalize the light curves and used the stitch attribute to create one continuous light curve for the 2 years of data we have (Figure 1b).

2.3. *Asteroseismic Analysis*

Once we had our light curves, we needed an asteroseismic analysis pipeline to estimate ν_{max} and $\Delta\nu$. For this purpose, we chose to use `pySYD` (Chontos et al. 2022) a new open-source python implementation of the effective and well-validated Sydney code (Huber et al. 2009). In addition to the automated analysis, `pySYD` has a feature to display figures of every processing step along the way. Because of this, we were able to visually inspect our results. Figure 2 shows a column from the complete `pySYD` final display. From the initial plotted power spectrum to the final echelle diagram, we can see that `pySYD` identified the oscillations of this star (TIC 25156036) and was able to calculate and present a correct ν_{max} and $\Delta\nu$ value. In the analysis, we tried varying the number of peaks in the autocorrelation function, the box filter width, and smoothing for the power spectrum. We found that none of these changes substantially impacted our results.

An echelle diagram is a plot of the frequency modulo the $\Delta\nu$ value, against the frequency (Figure 3a). In order to refine our estimates of the large frequency spacing, $\Delta\nu$, we used the echelle package HeyEchelle (Hey & Ball 2020) to make echelle diagrams for each of the stars. This package allows fine manual adjustments to the exact $\Delta\nu$ value until the ridges for the l=0, 1, and 2 modes line up exactly. We could search the $\Delta\nu$ given by `pySYD` and ±1 μHz around this value to double-check that we have the best $\Delta\nu$ possible. Using this option, we were able to try many $\Delta\nu$ values for one star and see how slight changes in our estimated value can improve our result (Figure 3b).

2.4. *Calibrations and Corrections*

2.4.1. *Scaling*

Once we had our finalized list of ν_{max} and $\Delta\nu$ for every star, we used these values to infer their seismic masses and radii. We used the modified version of the scaling relations (Kjeldsen & Bedding 1995), equations 1 and

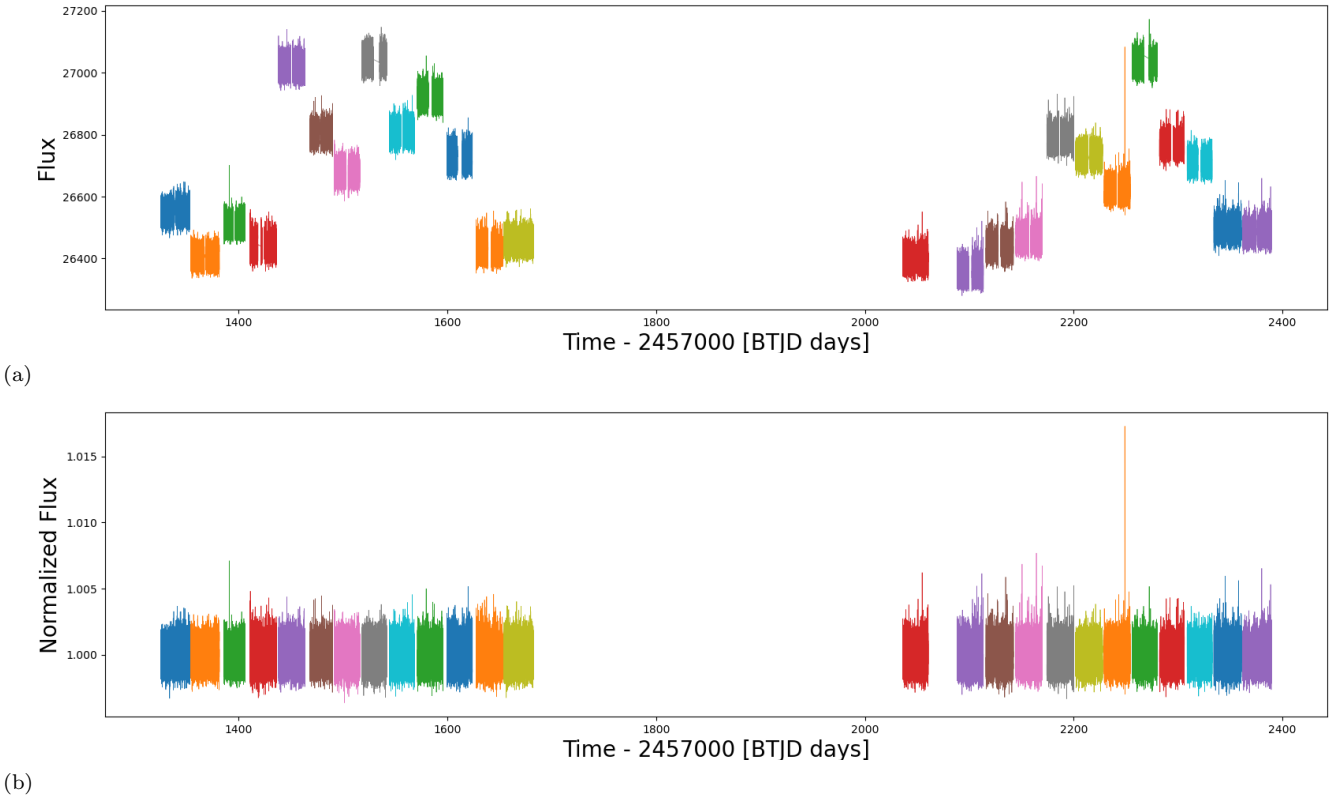

Figure 1. (**TOP**): Unedited time series for TIC 25156036. Before any normalizing or smoothing, we can see the differences in each sector, including sectors 1-13, 27, and 29-39. We show the totality of the two years of data that *TESS* provides, including the obvious discontinuities between sectors. Each sector is distinguished by a different color. (**BOTTOM**): The final normalized, smoothed, and stitched light curve. The sector colors are consistent between the two plots.

2 from Pinsonneault et al. (2018), and the solar values from the SYD pipeline from that same work, 3090 μHz for $\nu_{max,\odot}$ and 135.1 μHz for $\Delta\nu_{\odot}$.

$$\left(\frac{M_{sc}}{M_{\odot}}\right) = \left(\frac{\nu_{max}}{\nu_{max,\odot}}\right)^{3} \left(\frac{T_{eff}}{T_{eff,\odot}}\right)^{1.5} \left(\frac{\Delta\nu}{\Delta\nu_{\odot}}\right)^{-4} \quad (1)$$

$$\left(\frac{R_{sc}}{R_{\odot}}\right) = \left(\frac{\nu_{max}}{\nu_{max,\odot}}\right) \left(\frac{T_{eff}}{T_{eff,\odot}}\right)^{0.5} \left(\frac{\Delta\nu}{\Delta\nu_{\odot}}\right)^{-2} \quad (2)$$

2.4.2. *Corrections*

For each star in our sample, we also used a temperature from careful SED fitting (T_{eff} in Godoy-Rivera et al. 2021), and a $T_{eff,\odot}$ of 5777 K. Some of our stars in the SCVZ were independently analyzed in J. Tayar et al. (in prep) and so the uncertainties for ν_{max} and $\Delta\nu$ were calculated by taking the difference value between our values and the average value from previous works, i.e. Hatt et al. (2023), Lindsay et al. (2024), and J. Tayar et al. (in prep), and subtracting the average uncertainties from those previous works in quadrature. For the northern CVZ, we took the average fractional uncertainty from the southern CVZ and used that value for each star. We find that this compares well to other analyses of these stars (see Figure 5 in Section 3).

There are known deviations from the scaling relations (White et al. 2011). For our analysis, we estimate the theoretical $\Delta\nu$ correction for each of our stars using ASFGrid (Sharma et al. 2016; Stello & Sharma 2022) to find $f_{\Delta\nu}$. Specifically, we computed the correction using the ν_{max}, $\Delta\nu$, effective temperature, and [Fe/H] of each star. For the metallicity required in the grid, we used the Salaris correction (Salaris et al. 1993) calculated using a combination of the star's [M/H] and α-element enhancement, [α/Fe], from APOGEE Abdurro'uf et al. (2022), specifically the values from (Godoy-Rivera et al. 2021). This correction is included because enhancing α-elements in stars can increase opacity levels, thereby changing convection depths and subsequently altering oscillations. For the stars with no listed [Fe/H] value, we assumed solar metallicity [Fe/H]=0, which is roughly the average of our sample. Our total uncertainty on metallicity was then calculated by propagating forward the uncertainties on [M/H] from Godoy-Rivera et al. (2021), and [α/Fe] from APOGEE. Our $f_{\nu_{max}}$ correction was the multiplicative factor necessary to, on aver-

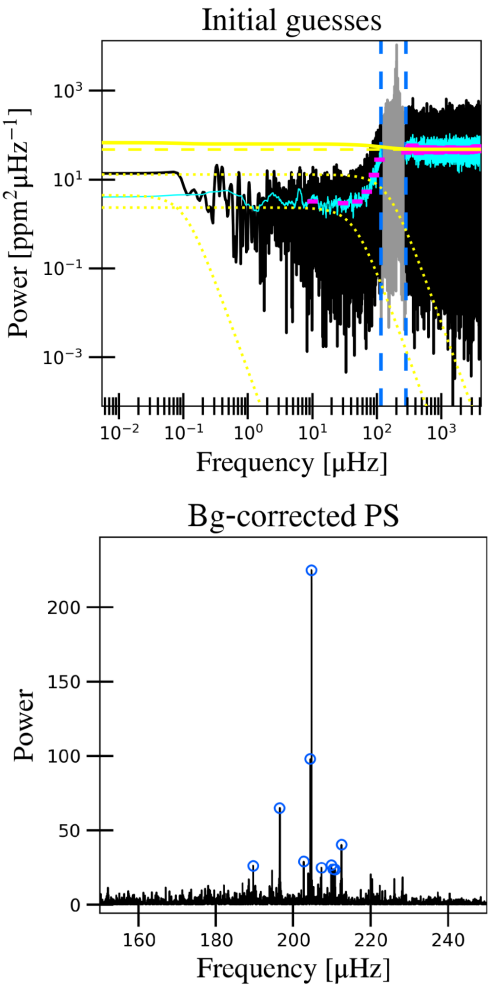

Figure 2. Output charts from `pySYD`. **(TOP)**: The power spectrum showing the area around ν_{max} (shaded region). We see a power excess caused by stellar oscillations (gray vertical band). The black shows the original power spectrum given by `pySYD` based on our given light curve. The blue shows a smoothed power spectrum and the pink shows a heavily smoothed power spectrum. The heavily smoothed power spectrum is used as an initial background fit to search for oscillations. We smoothed aggressively in the convective damping timescale to better see the star's oscillations and this resulted in low power at lower frequencies. **(BOTTOM)**: The corrected power spectrum with all smoothing removed showing a definite power excess in the same region.

age, have our seismically inferred luminosity match the luminosity from *Gaia*, with the uncertainty given by the propagated estimate of the scatter. Once we had both of our corrections, we can then use equations 3 and 4 to find our final corrected masses and radii (Tables 1).

$$M_{cor} = \frac{f^3_{\nu_{max}}}{f_{\Delta\nu}{}^4} M_{sc} \quad (3)$$

$$R_{cor} = \frac{f_{\nu_{max}}}{f_{\Delta\nu}{}^2} R_{sc} \quad (4)$$

3. VALIDATION

As described in the previous section, we used a combination of standard seismic analysis tools and visual inspection to identify and measure oscillation signatures. We used the data given by *Gaia* DR2 and the Apache Point Observatory Galactic Evolution Experiment (APOGEE) spectroscopic survey (Abdurro'uf et al. 2022) in order to check our seismic radii and surface gravities.

3.1. *Seismic Validation*

Previous asteroseismic analyses have included a subset of the stars we study here. For these stars in Figure 4a and 4b we show our ν_{max} and $\Delta\nu$ values compared directly to the ν_{max} and $\Delta\nu$ values from Hatt et al. (2023) and Lindsay et al. (2024). As expected, they are tightly correlated with only one of our stars differing greatly from Hatt et al. (2023). Given that this star's global parameters, validated with `pySYD`, align with our expectations regarding radius, mass, and surface gravity from external data, we have confidence that our star's ν_{max} value is a more accurate estimation for this star. We show a strong correlation between the seismic observables, ν_{max} and $\Delta\nu$, which is in line with other published literature (Figure 5). In general, we find that our ν_{max} and $\Delta\nu$ values are correlated in similar ways, suggesting reliable seismic measurements.

3.2. *Classical Validation*

We can also validate our results by direct comparison to results from classical methods. In Figures 6a and 6b, we show our seismic radii versus the radii derived from *Gaia* and our seismic surface gravities versus APOGEE's spectroscopic surface gravities as published in Godoy-Rivera et al. (2021). We find that they are generally well matched to the individually calibrated *Gaia* and APOGEE values listed in the Godoy-Rivera et al. (2021) paper with average uncertainties slightly lower at 0.059 dex for surface gravities and 0.23 $R_\odot$ for radii. Seismic radius uncertainties were calculated by propagating forward the uncertainties on the ν_{max}, $\Delta\nu$, T_{eff}, $f_{\nu_{max}}$, and $f_{\Delta\nu}$ according to standard error propagation. Surface gravity uncertainties were calculated by taking the Δlog(g) value between our seismic gravities and those from Godoy-Rivera et al. (2021) and subtracting the Godoy-Rivera et al. (2021) uncertainties in quadrature.

3.3. *Detection Probabilities*

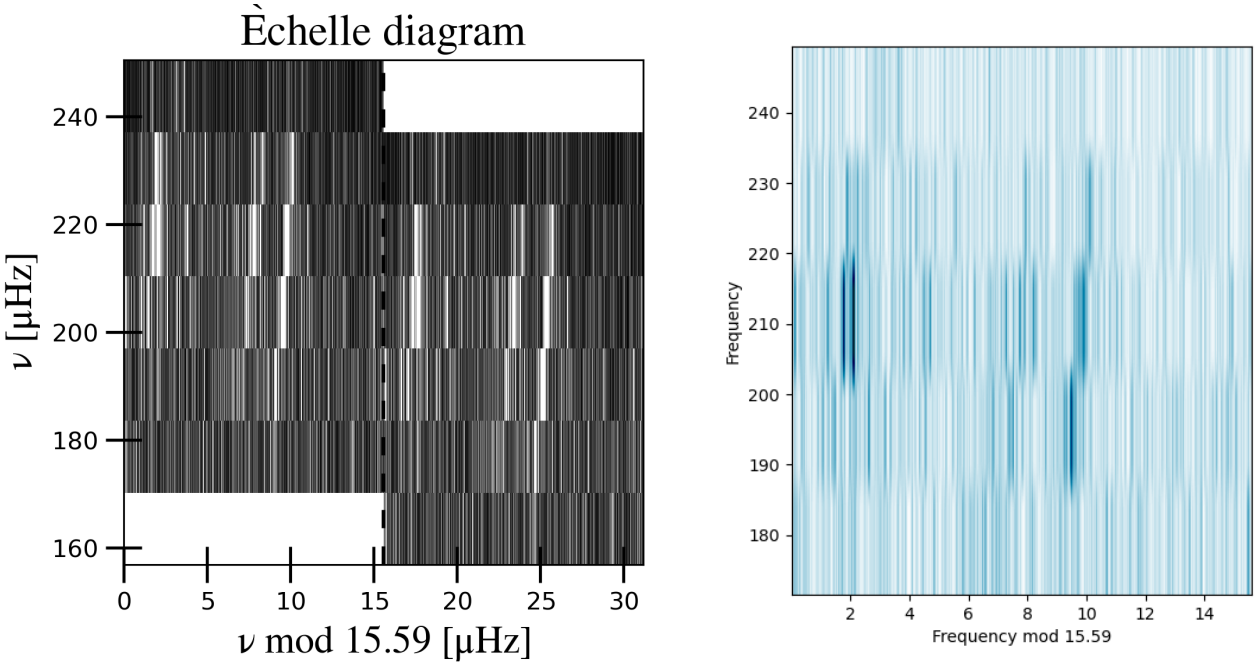

(a) (b)

Figure 3. (**LEFT**): Echelle diagram given by `pySYD` for TIC 25156036. With a $\Delta\nu$ of 15.59 μHz we can see ridges for the l=0, 1, and 2 modes. (**RIGHT**): Echelle diagram given by HeyEchelle for this same star, confirming the measured large frequency separation.

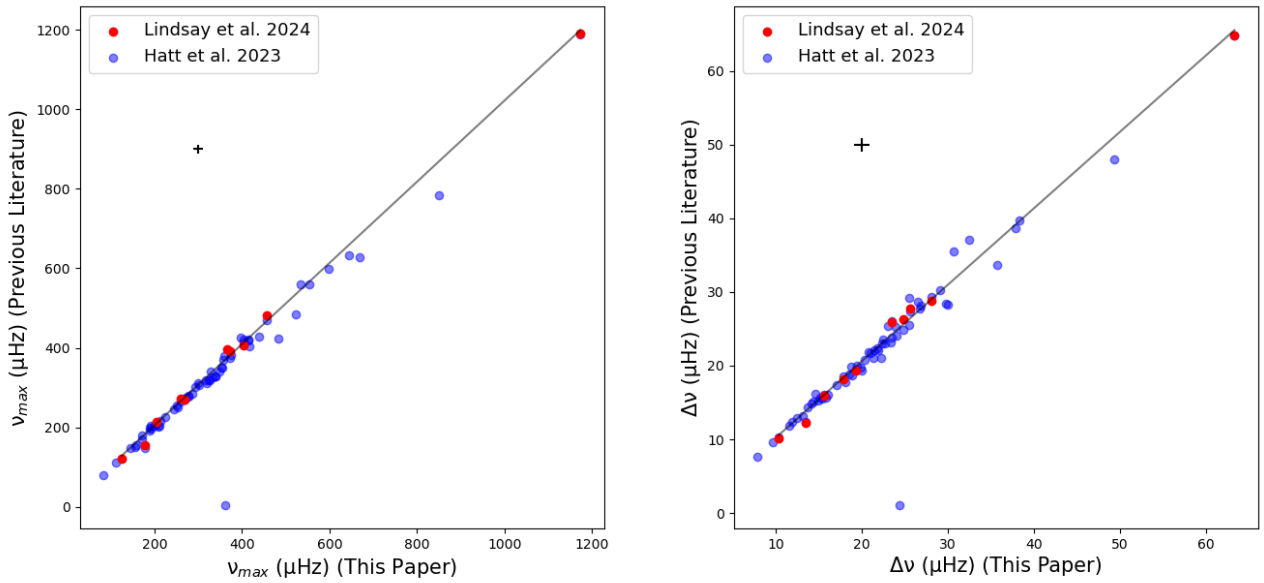

(a) (b)

Figure 4. Our ν_{max} values (left) and $\Delta\nu$ values (right) are consistent with previous work by Hatt et al. (2023) (blue) and Lindsay et al. (2024) (red). We show an overlapping subset of 66 stars out of our total 82 stars. We show an R^2 correlation value to Hatt et al. (2023) of 0.9918 and to Lindsay et al. (2024) of 0.9979. We find average offsets of 2.9% in ν_{max} and 3.7% in $\Delta\nu$, with no strong trends. Average error bars for the sample are shown in black in the top left corner.

The amplitudes and timescales of solar-like oscillations are expected to scale with the luminosities and temperatures of the stars. Predictions were made in Schofield et al. (2019) and Hey et al. (2024) about which

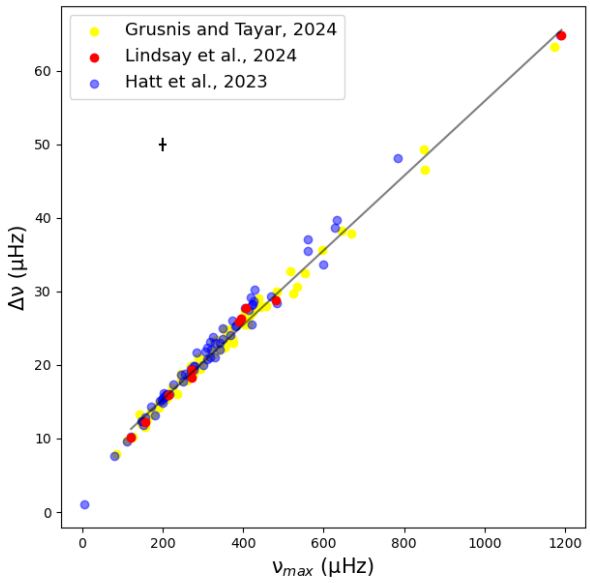

Figure 5. Linear relationship of ν_{max} vs $\Delta\nu$. Our unique star sample is shown in yellow compared to the samples that overlap with Hatt et al. (2023) in blue Lindsay et al. (2024) in red. Average error bars for the sample are shown in black in the top left corner.

stars in *TESS* should have detectable oscillations with a probability calculated using astrometric distances, magnitudes in the I and V bands, (B-V) color, sky position, and effective temperature. We show in Figure 7 a comparison between these predictions and our detections. In general, we find that the predictions in Schofield et al. (2019) and Hey et al. (2024) were overly optimistic. While the detection probabilities do correlate with detection rates, we detect oscillators in very few stars with a probability less than 70%. We can see a slight increase in prediction accuracy from the Hey et al. (2024) catalog versus the Schofield et al. (2019) catalog which could be because of the use of *Gaia* DR3 stellar parameters instead of values from *Gaia* DR2. It is also possible that with additional sectors or more careful light curve processing one could detect additional oscillators, but in general from the available light curves the noise seems to be higher than expected and therefore detections are less likely.

When plotting the *Gaia* Bp-Rp color versus the *Gaia* apparent G magnitude, we found that seismic detections in *TESS* subgiants are color and apparent magnitude dependent (Figure 8) with detections among early subgiants, which are bluer and fainter, tending to be rare. With short cadence data, we should be able to detect these oscillations. However, this color-magnitude trend implies that the noise level is too high, and it is possible that we would need the 20-second cadence data, which seems to have less noise (Huber et al. 2022) to actually identify these signals.

3.4. *Sample Distribution*

In Figure 9 we compare the luminosities and effective temperatures, derived in Godoy-Rivera et al. (2021), of the stars we detect oscillations for to those studied in *Kepler* (Serenelli et al. 2017; Pinsonneault et al. 2018). In general we find that our stars are more evolved than the well studied dwarfs (Serenelli et al. 2017) and less evolved than the well studied giants (Pinsonneault et al. 2018) as expected, filling in the region between these two *Kepler* samples.

Given their position on the HR diagram, we expected our seismic masses to fall within a range that was typical for stars on the subgiant branch, 0.9-1.6 $M_{\odot}$. After our corrections, we can see results that were consistent with these expectations, including a slight skew towards lower masses, likely coming from their longer time in this phase (Figure 10), with an uncertainty of 0.15 $M_{\odot}$. Seismic mass uncertainties were calculated, as previously mentioned for seismic radius, by propagating forward the uncertainties on the ν_{max}, $\Delta\nu$, T_{eff}, $f_{\nu_{max}}$, and $f_{\Delta\nu}$.

3.5. *Major Outlier: TIC 366490487*

For our sample, we found one major outlier, TIC 366490487. When completing the initial run through with `pySYD` star processing, we kept all of the stars that showed an oscillation bump and well-fit ν_{max} and $\Delta\nu$ values. One of these stars showed an excess of power not consistent with the expected Gaussian envelope (Figure 11). We examined the effects of looking at the Cycle 1 and Cycle 3 data for this star separately and found that while the same frequencies were present in each year, the amplitudes and amplitude ratios varied from year to year. Since there was still an excess of power in some capacity, we kept this star in our data table. However, for every validation figure, this particular star would be offset from the rest of the data if we assumed it was a solar-like oscillator. Because of this, we have left this star out of our final figures, but we include it here in case its behavior is interesting or relevant to other research.

4. COMPARING STELLAR MODELS

4.1. *Kiauhoku*

With our seismic masses and surface gravities, photometric effective temperatures, and corrected spectroscopic metallicities, we can utilize the `Kiauhoku` python package (Claytor et al. 2020) and compare a variety of public model grid's predictions to our measured values.

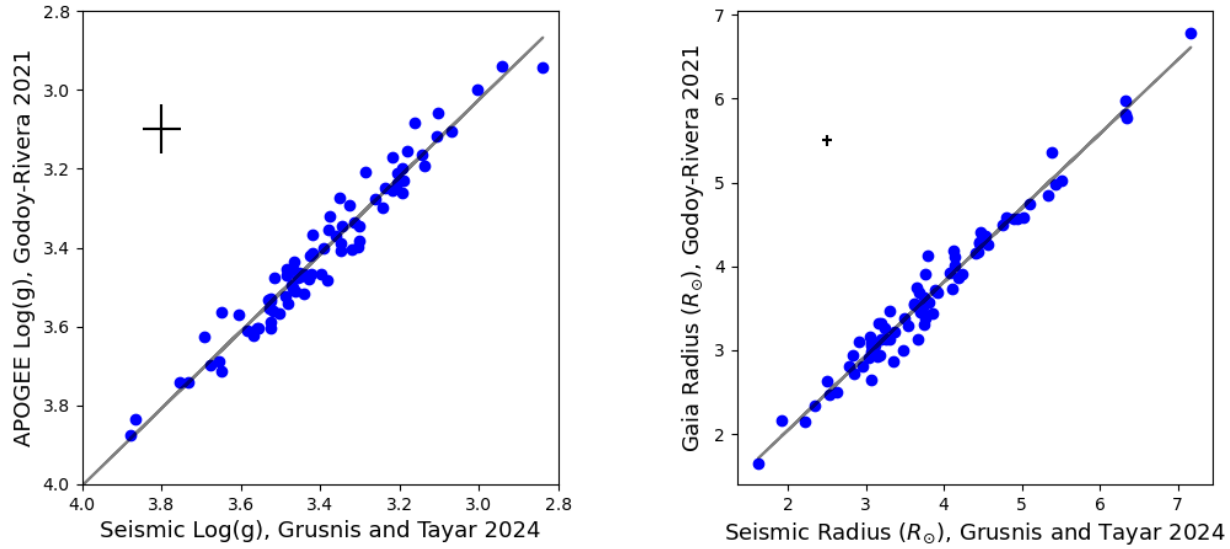

(a) (b)

Figure 6. Our seismic results compare well to spectroscopic surface gravities from APOGEE (left) and radii from *Gaia* (right, Godoy-Rivera et al. (2021). For each plot we show an average estimated uncertainty in the upper left corner.

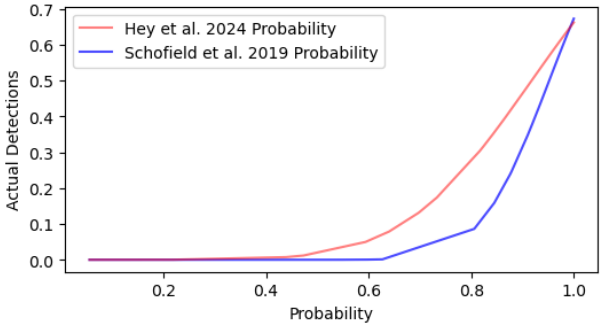

Figure 7. Cumulative distribution function for our solar-like oscillator detections versus the probability of detecting oscillators given by Schofield et al. (2019). Overall, the ranking of predictions was accurate, but we were less likely to detect oscillations than expected.

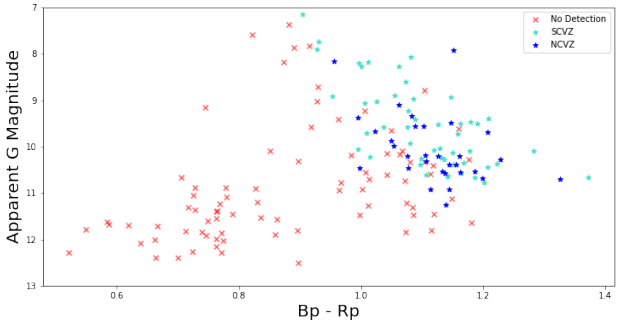

Figure 8. We show that there is a definite trend that brighter and redder stars are more likely to be detected as solar-like oscillators. Our SCVZ stars (light blue) that showed oscillations covered a wider range of colors but were brighter than the NCVZ oscillators (dark blue). The red x markers show stars with no detected oscillators.

Those comparisons show how well each model matches the data, and at what point they start to differ from these asteroseismic results.

4.2. *Models*

The models we used to compare to our seismic data were computed with the Modules for Experiments in Stellar Astrophysics (MESA) (Paxton et al. 2011) Isochrones and Stellar Tracks (MIST) (Choi et al. 2016), the Yale Rotating Stellar Evolution Code (YREC) (Pinsonneault et al. 1989) with the tracks from Tayar et al. (2022), the Garching Stellar Evolution Code (GARSTEC) (Weiss & Schlattl 2008) with tracks similar to Serenelli et al. (2013), and the Dartmouth Stellar Evolution Database (DSEP) (Dotter et al. 2008).

We chose these models because of their popularity and because they were all previously included in the `Kiauhoku` package. The MIST and DSEP stellar models are both made to cover a large range of stellar properties. The GARSTEC tracks have been often used for seismic analysis, and the YREC stellar model has an emphasis on helio- and asteroseismology and this set of tracks was particularly calibrated to the Pinsonneault et al. (2018) giants.

For our input parameters; mass, surface gravity, and metallicity, we set our prior search range to 0.001 $M_\odot$,

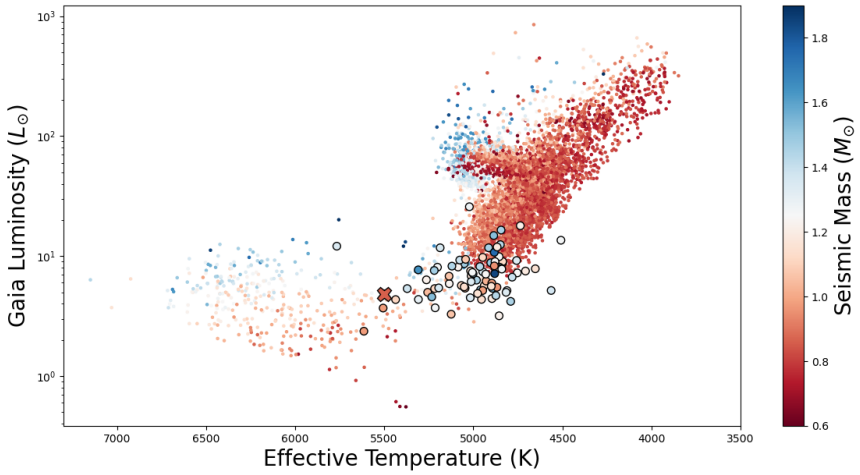

Figure 9. Asteroseismic masses as a function of temperature and luminosity. Our data is outlined with black circles and compared to previous result from *Kepler* for dwarfs (Serenelli et al. 2017), and giants (Pinsonneault et al. 2018). We also emphasize the location of one unusual star, TIC 366490487, see Section 3.5, with an x marker at a T_{eff} of 5499 K, and a luminosity of 4.84 $L_\odot$. In general, our seismic results are consistent with previous efforts, but populate a regime undersampled in *Kepler*.

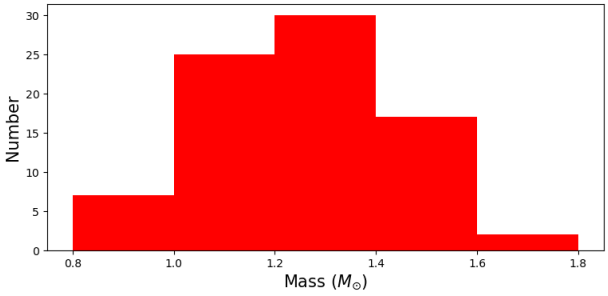

Figure 10. Mass distribution for our sample. As expected, these subgiants tend to be low mass stars ($1M_\odot - 1.3M_\odot$) near the solar age. The values range from 0.95-1.85 $M_\odot$, with an average uncertainty of 0.15 $M_\odot$.

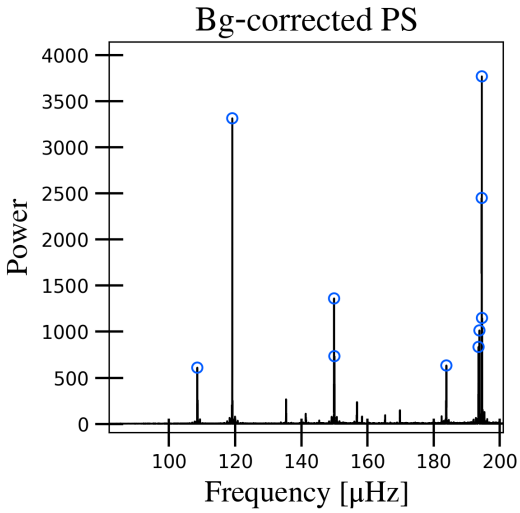

Figure 11. The background corrected power spectrum for TIC 366490487. Here we do not have a Gaussian envelope of power but instead we can see multiple large power spikes throughout a large range of frequencies.

0.001 dex, and 0.001 respectively, expecting the returned output parameters to fit better than this. This is consistent with previous `Kiauhoku` work, ensuring we were targeting our exact stars. We then took the difference in our effective temperature and the model's effective temperature and plotted that against surface gravity. We have removed the 5 outlying stars so Figure 12 is focused on the best fits from ΔT_{eff} of -500 to 500 K. On average, the models differed by about ± 120K from our data. All of the models gave fairly consistent results for both model offsets and inferred ages.

4.3. *Results*

At log(g) between 2.8 and 3.6, we found that the difference in T_{eff} between the data and the models was fairly low, with an average of ± 120K from our data. However, when including log(g) values greater than 3.6, the average difference in T_{eff} rose to about ± 340 K.

These offsets show that the stellar model grids are roughly consistent with, but not exactly calibrated to, giant stars, with a trend of predicting that they will be hotter than what we observe. For the true subgiant stars, the models are not very accurate, with the average difference almost triple what it was for the lower giants. The scatter between the points also increases, meaning it would be much more challenging to calibrate sub-

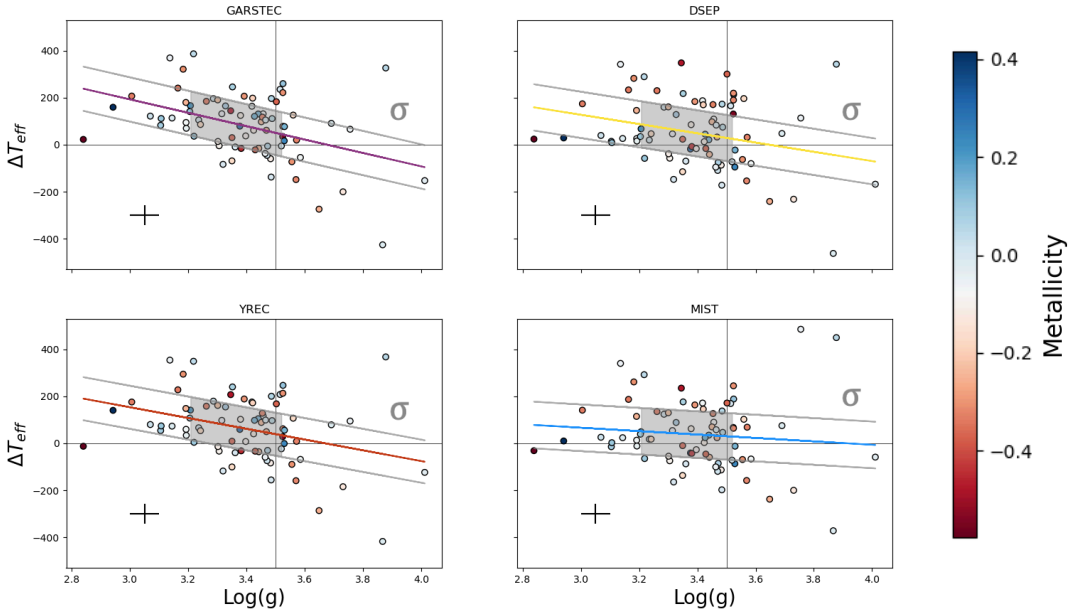

Figure 12. Surface gravity versus the temperature difference between the model and our observables, color coded by metallicity, for each set of models: GARSTEC, DSEP, YREC, and MIST. The first gray line from the linear regression line shows a 1σ error. The gray box is showing where the bulk of the data is. The horizontal line is at $\Delta T_{eff} = 0$ and the vertical line is at $log(g) = 3.5$ roughly separating the giants on the left and the subgiants on the right. Our observed errors are shown in the bottom left corner of each subplot.

giant stellar models to photometric and spectroscopic data we have already. More generally, we expect that stellar models need to be improved for all evolutionary stages, and especially for transition stages like the subgiant stage where the changes in the internal structure of a star are much more pronounced.

4.4. *Ages*

Alongside our ability to compare our surface gravities and effective temperatures with those of the models, we were also able to compute age estimates for all of our stars, using each set of models. We found that the age estimates for each star were relatively similar between all four of the models so we chose to only display the results from the MIST model for clarity (Figure 13). The MIST model had the lowest average temperature difference with our data at $\pm 106K$, while the other three models had an average difference of about $\pm 120K$. The standard deviation from the linear regression line for GARSTEC, DSEP, YREC, and MIST was 94 K, 99 K, 92 K, and 99 K respectively and the average difference in temperature for each individual star across the models was relatively low ($\pm 42K$).

The ages range from about 1.2-21.2 Gyr, with the bulk of our stars from 1.2-9.6 Gyr with an average observational uncertainty of 0.54 Gyr. In our histogram in Figure 13, we show our ages compared with the ages given by Serenelli et al. (2017). We observe that the ages of our stars predicted by the models align with those of nearby stars observed by *Kepler*, affirming that our asteroseismic findings allow us to estimate ages that are consistent with earlier studies. Thus, this asteroseismic work, as well as future works, can be combined and used to further our understanding of galactic formation and evolution.

4.4.1. *Age Conclusions*

We used our metallicities and the alpha-enhancement parameter, [α/M], to look for trends between age and composition. We show the results for MIST in Figures 14 and 15.

In Figure 14a, we show the APOGEE metallicities versus the ages using MIST. We see no strong trends between [M/H] and age in this regime, reinforcing that [M/H] cannot be used as an age indicator for metal-rich populations.

Most of stars are between the ages of 1.2 and 9.6 Gyr, which is as expected for a thin disk, alpha-poor population, with the median age of 3.7 Gyr. However, 6 of our 82 stars turned out much higher in age than the typical range for subgiant stars. In Figure 14a, it is shown that the metallicities for these 6 stars are typical, ranging from about -0.3 to 0.2, and they were well fit by our modeling. This is not the first time something like this has been seen. For example, Stassun et al. (2009) shows how eclipsing binaries give very accurate physical

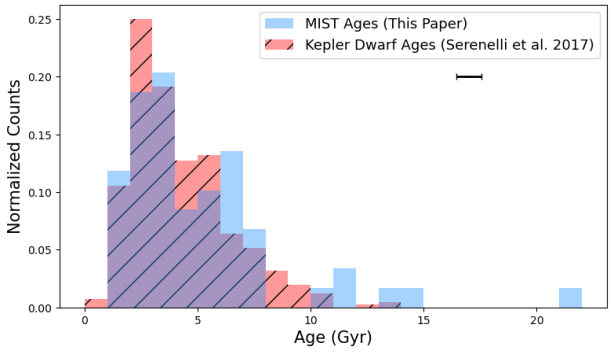

Figure 13. Age estimates from the MIST stellar model tracks. We show our ages (blue) normalized in comparison to the ages from Serenelli et al. (2017) (red) and can see that the ages for the *TESS* stars are quite consistent with previous studies from *Kepler*, perhaps because both sample a local population. We note at least one star whose age is not consistent with the age of the universe suggesting that it likely experienced mass loss perhaps due to a close binary companion. The average observed error bar is in the upper right corner.

property values, but the ages can show these stars to be 50-90% older than their actual age. This happens when a close binary system strips mass from its counterpart, leading to a less massive subgiant than what a star that age would normally be, so we suggest that these stars may have undergone mass loss because of an interaction with a binary companion. In Figure 14b, we show no strong correlation between the ages of our stars and their α-element enhancement. We see the same 6 outliers. We also identify 5 stars that would be classified as young α rich stars by Martig et al. (2015). It has been suggested that these could either result from recent formation of stars from α-enriched gas or that they could be the result of mass gain from close interaction with a binary companion, making them appear younger than they actually are (Chiappini et al. 2015; Jofré et al. 2023). We expect that the existence and frequency of such stars before the giant branch could be helpful in illuminating the dominant formation mechanism.

Figure 15 shows [α/M] plotted against [M/H] color-coded by age. The gray points in the background are stars from APOGEE DR17 in the same metallicity and temperature regime as our sample. With this underlay of data, we can see that many of our stars fall on the alpha-poor (thin-disk) band, although we do have a few stars lying on the alpha-rich (thick-disk) band. Comparing our ages to those expected from galactic chemical enrichment models, we notice both young α rich stars as well as at least one star that is very old and α poor. The number of age outliers in key places makes it challenging to place strong chemical enrichment constraints from just this small sample, but we suggest that larger samples of stars like this could be helpful in understanding the chemical evolution of the Milky Way.

5. DISCUSSIONS AND CONCLUSIONS

In this paper, we present a detailed first look at the oscillating subgiants and lower giants from the *TESS* Northern and Southern CVZs. We show that two years of data is sufficient to measure the precise ν_{max} and $\Delta\nu$ parameters for these stars, and compute seismic radii, masses, surface gravities, and ages. We present seismic results for 82 stars, with masses ranging from 0.95-1.85 $M_{\odot}$ with average uncertainties of 0.15 $M_{\odot}$, radii ranging from 1.62-7.17 $R_{\odot}$ with an uncertainty of 0.23 $R_{\odot}$, and surface gravities ranging from 2.94-4.02 dex with an uncertainty of approximately 0.059 dex. These results presented here are shown to be consistent with previous results, including those from other seismic studies, spectroscopy, and *Gaia*.

We demonstrated in Section 4 how a sample like this can be used to test and validate stellar models. We compare them to several public model grids in this regime. In general, we found that the models provided predictions that are similar to each other and similar to the data, although we note some slight offsets and trends with surface gravity. We also showed that this sample of stars probes a range of ages, compositions, and galactic populations including young alpha-enhanced, alpha-rich, and alpha-poor disks.

We expect this sample to be useful for a variety of future investigations including the calibration of spectroscopic surface gravity values (Hekker et al. 2013; Liu et al. 2015), identifying stars for He analysis (Lindsay et al. 2024), checking stellar models in this region (Geller et al. 2017; Schutte et al. 2022; Li et al. 2020a), estimating ages and age distributions (Xiang & Rix 2022), and analyzing core rotation (Deheuvels et al. 2012; Mosser et al. 2012). More generally, using *TESS* data for asteroseismology is an effective way to get precise and accurate stellar parameters. As more data is gathered on stellar oscillations, we will have a greater ability to understand structures and compositions of stars along with interesting and important details like convective mixing and magnetic activity within stellar interiors.

ACKNOWLEDGEMENTS

We thank Ashley Chontos for helpful discussions about using the `pySYD` package. We thank Zachary Claytor for help with HiperGator. We thank Sarbani Basu for helpful suggestions. We thank Christopher Lindsay and Joel Ong for sending their ν_{max} and $\Delta\nu$ values for comparison in this paper.

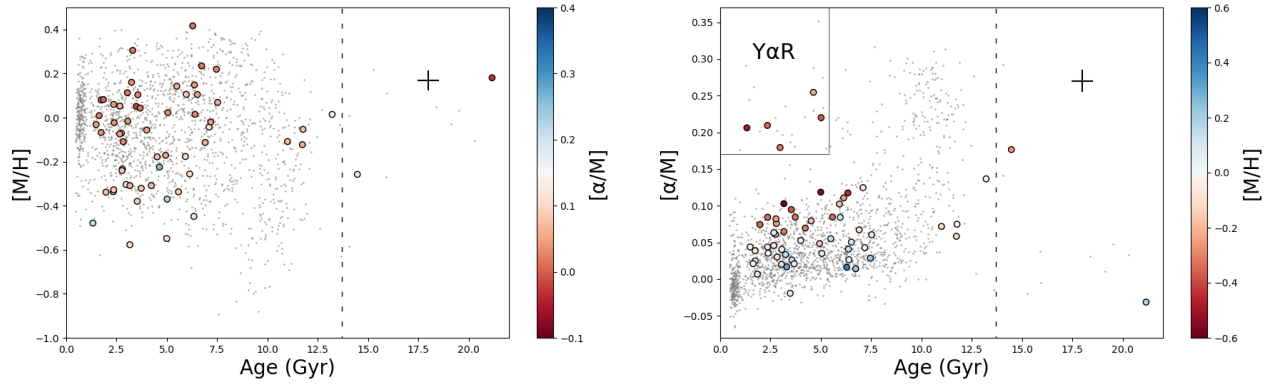

(a) (b)

Figure 14. (LEFT): [M/H] plotted against ages given by the MIST stellar models. We see no strong correlation between [M/H] and age. **(RIGHT)**: [α/M] plotted against ages given by the MIST stellar model. In the top left corner, we can see our young alpha-enhanced (yαr) stars. The α-rich, thick disk stars are in the top right quadrant, with the remaining lower half of the chart representing the thin disk. Most of the sample are low-alpha stars.The dotted line shows the age of the universe for reference.

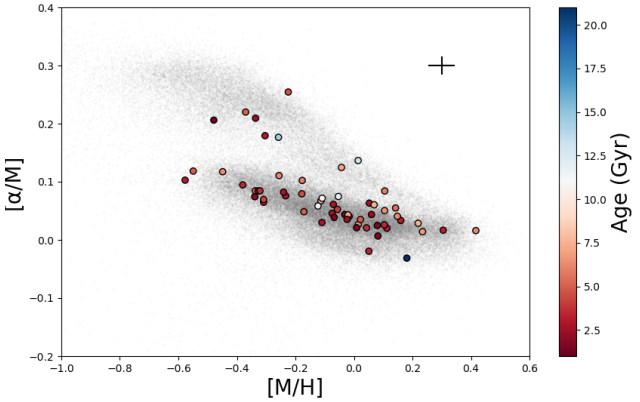

Figure 15. [α/M] plotted against [M/H]. Our data is circled in black and color-coded by age. We show for comparison (gray) the full sample from the APOGEE DR17 spectroscopic survey in this temperature and metallicity regime. Average error bars are shown in the top right corner.

SG and JT acknowledge support from NASA grants 80NSSC23K0143 and 80NSSC23K0436. JT also acknowledges support from NASA grants 80NSSC20K0056 and 80NSSC19K0367.

This work has made use of data from the European Space Agency (ESA) mission *Gaia* (https://www.cosmos.esa.int/gaia), processed by the *Gaia* Data Processing and Analysis Consortium (DPAC, https://www.cosmos.esa.int/web/gaia/dpac/consortium). Funding for the DPAC has been provided by national institutions, in particular the institutions participating in the *Gaia* Multilateral Agreement.

Funding for the Sloan Digital Sky Survey IV has been provided by the Alfred P. Sloan Foundation, the U.S. Department of Energy Office of Science, and the Participating Institutions.

SDSS-IV acknowledges support and resources from the Center for High Performance Computing at the University of Utah. The SDSS website is www.sdss4.org.

SDSS-IV is managed by the Astrophysical Research Consortium for the Participating Institutions of the SDSS Collaboration including the Brazilian Participation Group, the Carnegie Institution for Science, Carnegie Mellon University, Center for Astrophysics — Harvard & Smithsonian, the Chilean Participation Group, the French Participation Group, Instituto de Astrofísica de Canarias, The Johns Hopkins University, Kavli Institute for the Physics and Mathematics of the Universe (IPMU) / University of Tokyo, the Korean Participation Group, Lawrence Berkeley National Laboratory, Leibniz Institut für Astrophysik Potsdam (AIP), Max-Planck-Institut für Astronomie (MPIA Heidelberg), Max-Planck-Institut für Astrophysik (MPA Garching), Max-Planck-Institut für Extraterrestrische Physik (MPE), National Astronomical Observatories of China, New Mexico State University, New York University, University of Notre Dame, Observatário Nacional / MCTI, The Ohio State University, Pennsylvania State University, Shanghai Astronomical Observatory, United Kingdom Participation Group, Universidad Nacional Autónoma de México, University of Arizona, University of Colorado Boulder, University of Oxford, University of Portsmouth, University of Utah, University of Virginia, University of Washington, University of Wisconsin, Vanderbilt University, and Yale University.

Transiting Exoplanet Survey Satellite (TESS) was accessed on DATE from https://registry.opendata.aws/tess. This paper includes data collected with the *TESS* mission, obtained from the AWS Open Data copy of the MAST Archive at the Space Telescope Science Institute

(STScI). Funding for the *TESS* mission is provided by the NASA Explorer Program. STScI is operated by the Association of Universities for Research in Astronomy, Inc., under NASA contract NAS 5–26555.

Software: `Kiauhoku` (**Claytor et al. 2020**), `NumPy` (**Harris et al. 2020**), `Lightkurve` (**Lightkurve Collaboration et al. 2018**), `AstroPy` (**Astropy Collaboration et al. 2013, 2018, 2022**), `Matplotlib` (**Hunter 2007**), `SciPy` (**Virtanen et al. 2020**), `pySYD` (**Chontos et al. 2022**), `HeyEchelle` (**Hey & Ball 2020**), `Pandas` (**McKinney 2010**), `ASFGrid` (**Sharma & Stello 2016**)

REFERENCES

Abdurro'uf, Accetta, K., Aerts, C., et al. 2022, ApJS, 259, 35, doi: 10.3847/1538-4365/ac4414

Aerts, C., Christensen-Dalsgaard, J., & Kurtz, D. W. 2010, Asteroseismology, doi: 10.1007/978-1-4020-5803-5

Astropy Collaboration, Robitaille, T. P., Tollerud, E. J., et al. 2013, A&A, 558, A33, doi: 10.1051/0004-6361/201322068

Astropy Collaboration, Price-Whelan, A. M., Sipőcz, B. M., et al. 2018, AJ, 156, 123, doi: 10.3847/1538-3881/aabc4f

Astropy Collaboration, Price-Whelan, A. M., Lim, P. L., et al. 2022, ApJ, 935, 167, doi: 10.3847/1538-4357/ac7c74

Bedding, T. R., & Kjeldsen, H. 2022, Research Notes of the American Astronomical Society, 6, 202, doi: 10.3847/2515-5172/ac8f94

Bedding, T. R., Huber, D., Stello, D., et al. 2010, ApJL, 713, L176, doi: 10.1088/2041-8205/713/2/L176

Chiappini, C., Anders, F., Rodrigues, T. S., et al. 2015, A&A, 576, L12, doi: 10.1051/0004-6361/201525865

Choi, J., Dotter, A., Conroy, C., et al. 2016, ApJ, 823, 102, doi: 10.3847/0004-637X/823/2/102

Chontos, A., Huber, D., Sayeed, M., & Yamsiri, P. 2022, The Journal of Open Source Software, 7, 3331, doi: 10.21105/joss.03331

Claytor, Z. R., van Saders, J. L., Santos, Â. R. G., et al. 2020, ApJ, 888, 43, doi: 10.3847/1538-4357/ab5c24

Deheuvels, S., García, R. A., Chaplin, W. J., et al. 2012, ApJ, 756, 19, doi: 10.1088/0004-637X/756/1/19

Deheuvels, S., Doğan, G., Goupil, M. J., et al. 2014, A&A, 564, A27, doi: 10.1051/0004-6361/201322779

do Nascimento, J. D., da Costa, J. S., & Castro, M. 2012, A&A, 548, L1, doi: 10.1051/0004-6361/201219791

Dotter, A., Chaboyer, B., Jevremović, D., et al. 2008, ApJS, 178, 89, doi: 10.1086/589654

Fritzewski, D. J., Van Reeth, T., Aerts, C., et al. 2024, A&A, 681, A13, doi: 10.1051/0004-6361/202347618

García, R. A., Mathur, S., Pires, S., et al. 2014, A&A, 568, A10, doi: 10.1051/0004-6361/201323326

Geller, A. M., Leiner, E. M., Chatterjee, S., et al. 2017, ApJ, 842, 1, doi: 10.3847/1538-4357/aa72ef

Gilliland, R. L. 2011, in Astronomical Society of the Pacific Conference Series, Vol. 448, 16th Cambridge Workshop on Cool Stars, Stellar Systems, and the Sun, ed. C. Johns-Krull, M. K. Browning, & A. A. West, 167

Gilliland, R. L., Brown, T. M., Christensen-Dalsgaard, J., et al. 2010, PASP, 122, 131, doi: 10.1086/650399

Godoy-Rivera, D., Tayar, J., Pinsonneault, M. H., et al. 2021, ApJ, 915, 19, doi: 10.3847/1538-4357/abf8ba

Harris, C. R., Millman, K. J., van der Walt, S. J., et al. 2020, Nature, 585, 357, doi: 10.1038/s41586-020-2649-2

Hatt, E., Nielsen, M. B., Chaplin, W. J., et al. 2023, A&A, 669, A67, doi: 10.1051/0004-6361/202244579

Hekker, S., Elsworth, Y., Mosser, B., et al. 2013, A&A, 556, A59, doi: 10.1051/0004-6361/201321630

Hey, D., & Ball, W. 2020, Echelle: Dynamic echelle diagrams for asteroseismology, 1.4, Zenodo, doi: 10.5281/zenodo.3629933

Hey, D., Huber, D., Ong, J., Stello, D., & Foreman-Mackey, D. 2024, arXiv e-prints, arXiv:2403.02489, doi: 10.48550/arXiv.2403.02489

Higl, J., & Weiss, A. 2017, A&A, 608, A62, doi: 10.1051/0004-6361/201731008

Hon, M., Bellinger, E. P., Hekker, S., Stello, D., & Kuszlewicz, J. S. 2020, MNRAS, 499, 2445, doi: 10.1093/mnras/staa2853

Huber, D., Stello, D., Bedding, T. R., et al. 2009, Communications in Asteroseismology, 160, 74, doi: 10.48550/arXiv.0910.2764

Huber, D., Chaplin, W. J., Chontos, A., et al. 2019, AJ, 157, 245, doi: 10.3847/1538-3881/ab1488

Huber, D., White, T. R., Metcalfe, T. S., et al. 2022, AJ, 163, 79, doi: 10.3847/1538-3881/ac3000

Hunter, J. D. 2007, Computing in Science & Engineering, 9, 90, doi: 10.1109/MCSE.2007.55

Jofré, P., Jorissen, A., Aguilera-Gómez, C., et al. 2023, A&A, 671, A21, doi: 10.1051/0004-6361/202244524

Kalirai, J. S., & Richer, H. B. 2010, Philosophical Transactions of the Royal Society of London Series A, 368, 755, doi: 10.1098/rsta.2009.0257

Kjeldsen, H., & Bedding, T. R. 1995, A&A, 293, 87, doi: 10.48550/arXiv.astro-ph/9403015

Li, T., Bedding, T. R., Christensen-Dalsgaard, J., et al. 2020a, MNRAS, 495, 3431, doi: 10.1093/mnras/staa1350
Li, Y., Bedding, T. R., Li, T., et al. 2020b, MNRAS, 495, 2363, doi: 10.1093/mnras/staa1335
Lightkurve Collaboration, Cardoso, J. V. d. M., Hedges, C., et al. 2018, Lightkurve: Kepler and TESS time series analysis in Python, Astrophysics Source Code Library. http://ascl.net/1812.013
Lindegren, L., Lammers, U., Bastian, U., et al. 2016, A&A, 595, A4, doi: 10.1051/0004-6361/201628714
Lindegren, L., Hernández, J., Bombrun, A., et al. 2018, A&A, 616, A2, doi: 10.1051/0004-6361/201832727
Lindsay, C. J., Ong, J. M. J., & Basu, S. 2024, ApJ, 965, 171, doi: 10.3847/1538-4357/ad2ae5
Liu, C., Fang, M., Wu, Y., et al. 2015, ApJ, 807, 4, doi: 10.1088/0004-637X/807/1/4
Martig, M., Rix, H.-W., Silva Aguirre, V., et al. 2015, MNRAS, 451, 2230, doi: 10.1093/mnras/stv1071
McKinney, W. 2010, in Proceedings of the 9th Python in Science Conference, ed. S. van der Walt & J. Millman, 51 – 56
Mosser, B., Goupil, M. J., Belkacem, K., et al. 2012, A&A, 548, A10, doi: 10.1051/0004-6361/201220106
Mosser, B., Benomar, O., Belkacem, K., et al. 2014, A&A, 572, L5, doi: 10.1051/0004-6361/201425039
Paxton, B., Bildsten, L., Dotter, A., et al. 2011, ApJS, 192, 3, doi: 10.1088/0067-0049/192/1/3
Pinsonneault, M. H., Kawaler, S. D., Sofia, S., & Demarque, P. 1989, ApJ, 338, 424, doi: 10.1086/167210
Pinsonneault, M. H., Elsworth, Y. P., Tayar, J., et al. 2018, ApJS, 239, 32, doi: 10.3847/1538-4365/aaebfd
Quirion, P.-O., Christensen-Dalsgaard, J., & Arentoft, T. 2010, ApJ, 725, 2176, doi: 10.1088/0004-637X/725/2/2176
Rendle, B. M., Buldgen, G., Miglio, A., et al. 2019, MNRAS, 484, 771, doi: 10.1093/mnras/stz031
Ricker, G. R., Winn, J. N., Vanderspek, R., et al. 2015, Journal of Astronomical Telescopes, Instruments, and Systems, 1, 014003, doi: 10.1117/1.JATIS.1.1.014003
Rodrigues, T. S., Bossini, D., Miglio, A., et al. 2017, MNRAS, 467, 1433, doi: 10.1093/mnras/stx120
Salaris, M., Chieffi, A., & Straniero, O. 1993, ApJ, 414, 580, doi: 10.1086/173105
Schofield, M., Chaplin, W. J., Huber, D., et al. 2019, ApJS, 241, 12, doi: 10.3847/1538-4365/ab04f5
Schutte, M. C., Hebb, L., Lowry, S., et al. 2022, AJ, 164, 14, doi: 10.3847/1538-3881/ac70ca
Serenelli, A., Johnson, J., Huber, D., et al. 2017, ApJS, 233, 23, doi: 10.3847/1538-4365/aa97df
Serenelli, A. M., Bergemann, M., Ruchti, G., & Casagrande, L. 2013, MNRAS, 429, 3645, doi: 10.1093/mnras/sts648
Sharma, S., & Stello, D. 2016, Asfgrid: Asteroseismic parameters for a star, Astrophysics Source Code Library, record ascl:1603.009
Sharma, S., Stello, D., Bland-Hawthorn, J., Huber, D., & Bedding, T. R. 2016, ApJ, 822, 15, doi: 10.3847/0004-637X/822/1/15
Sreenivas, K. R., Bedding, T. R., Li, Y., et al. 2024, arXiv e-prints, arXiv:2401.17557, doi: 10.48550/arXiv.2401.17557
Stassun, K. G., Hebb, L., López-Morales, M., & Prša, A. 2009, in The Ages of Stars, ed. E. E. Mamajek, D. R. Soderblom, & R. F. G. Wyse, Vol. 258, 161–170, doi: 10.1017/S1743921309031810
Stello, D., & Sharma, S. 2022, Research Notes of the American Astronomical Society, 6, 168, doi: 10.3847/2515-5172/ac8b12
Tayar, J., Claytor, Z. R., Huber, D., & van Saders, J. 2022, ApJ, 927, 31, doi: 10.3847/1538-4357/ac4bbc
Virtanen, P., Gommers, R., Oliphant, T. E., et al. 2020, Nature Methods, 17, 261, doi: 10.1038/s41592-019-0686-2
Weiss, A., & Schlattl, H. 2008, Ap&SS, 316, 99, doi: 10.1007/s10509-007-9606-5
White, T. R., Bedding, T. R., Stello, D., et al. 2011, ApJ, 743, 161, doi: 10.1088/0004-637X/743/2/161
Xiang, M., & Rix, H.-W. 2022, Nature, 603, 599, doi: 10.1038/s41586-022-04496-5
Xiang, M., Liu, X., Shi, J., et al. 2017, ApJS, 232, 2, doi: 10.3847/1538-4365/aa80e4
Zhou, J., Bi, S., Yu, J., et al. 2024, ApJS, 271, 17, doi: 10.3847/1538-4365/ad18db

Table 1. Seismic Values and Uncertainties

TIC ID	ν_{max}	$\Delta\nu$	$f_{\Delta\nu}$	$log(g)$	M_{cor}	R_{cor}	Age	T_{eff}	[M/H]	$[\alpha/M]$	$\sigma_{\nu_{max}}$	$\sigma_{\Delta\nu}$	$\sigma_{log(g)}$	$\sigma_{M_{cor}}$	$\sigma_{R_{cor}}$	σ_{Age}	$\sigma_{T_{eff}}$	$\sigma_{[M/H]}$	$\sigma_{\alpha/M}$
	[μHz]	[μHz]	-	[dex]	[$M_\odot$]	[$R_\odot$]	[Gyr]	[K]	-	-	[μHz]	[μHz]	[dex]	[$M_\odot$]	[$R_\odot$]	[Gyr]	[K]	-	-
25156036	202.34	15.64	0.985	3.21	1.16	4.46	7.46	4652	0.22	0.029	4.39	0.23	0.064	0.16	0.06	0.42	24	0.0057	0.0045
31506424	396.06	26.49	1.015	3.52	1.11	3.04	4.99	5217	-0.55	0.118	17.65	2.20	0.062	0.02	0.12	0.50	26	0.0096	0.11
38602419	438.48	29.11	1.016	3.57	1.04	2.79	7.49	5256	-0.32	0	8.56	0.77	0.005	0.11	0.03	0.95	43.5	0.0158	0
41587424	190.19	14.18	0.999	3.19	1.46	5.11	2.74	4914	-0.07	0.061	7.77	0.90	0.076	0.14	0.33	0.28	29	0.0069	0.0056
55270123	365.31	22.07	1.006	3.48	1.11	3.19	6.9	5067	-0.11	0.067	15.51	1.40	0.021	0.11	0.04	0.71	23	0.0074	0.0059
141335100	111.5	9.69	0.984	2.94	1.26	6.33	6.28	4508	0.42	0.016	0.68	0.14	0.065	0.09	0.31	0.27	16	0.005	0.0038
141626634	506.76	30.63	1.017	3.65	1.86	3.46	1.29	5309	0	0	28.98	1.24	0.072	0.10	0.12	0.14	34.5	0.01	0
141757732	178.81	13.43	0.994	3.16	1.53	5.39	1.97	4885	-0.34	0.074	22.46	1.06	0.017	0.09	0.15	0.21	16	0.0082	0.0069
142109390	374.3	26.18	1.008	3.48	1.55	3.75	2.35	4892	0.06	0.044	8.72	2.49	0.061	0.33	0.44	0.23	21.5	0.0064	0.0051
149390710	333.49	23.43	1.010	3.44	1.05	3.25	7.77	5046	-0.24	0	3.48	0.20	0.038	0.11	0.11	1.00	26.5	0.0396	0
150030411	413.97	24.91	0.994	3.53	1.19	3.12	6.73	4895	0.23	0.014	12.10	1.30	0.053	0.15	0.15	0.32	22.5	0.0057	0.0406
150062447	643.99	41.12	1.015	3.73	0.8	2.03	20.44	5124	-0.13	0	5.42	1.29	0.045	0.09	0.03	2.99	34	0.0013	0
150166759	204.12	16.4	1.005	3.22	1.18	4.45	6.52	4836	0.1	0.05	4.31	0.42	0.064	0.19	0.16	0.49	21.5	0.006	0.0049
150393198	192.08	14.94	1.015	3.19	1.12	4.46	7.1	4835	-0.04	0.125	3.81	0.16	0.019	0.17	0.15	0.76	17	0.0064	0.0053
150430044	292.74	20.56	0.999	3.38	1.47	4.13	3.3	4852	0.31	0.017	3.40	0.78	0.044	0.13	0.09	0.14	17.5	0.0056	0.0043
150442152	260.06	17.27	0.995	3.33	1.72	4.74	1.74	4902	0.08	0.025	10.00	0.40	0.066	0.17	0.25	0.16	26	0.0064	0.0129
167342488	347.35	22.38	1.001	3.46	1.46	3.76	2.66	4982	-0.07	0.046	7.69	0.64	0.063	0.10	0.37	0.31	19.5	0.0072	0.0057
167548586	373.62	23.5	0.999	3.49	1.49	3.66	2.66	4959	0.05	0.063	6.87	2.48	0.052	0.24	0.54	0.26	28.5	0.0065	0.0052
177241155	191.08	15.88	1.007	3.19	1.26	4.75	4.09	4855	-0.25	0	15.70	1.47	0.064	0.21	0.24	0.47	18.5	0.0127	0
220457103	319.26	21.81	1.014	3.43	1.27	3.62	3.53	5201	-0.38	0.095	5.97	0.44	0.030	0.13	0.03	0.40	17.5	0.0091	0.12
257720189	361.37	24.4	1.005	3.47	1.12	3.24	7.52	4938	0.07	0.06	183.09	11.92	0.058	0.14	0.04	0.66	16.5	0.0063	0.0469
260078030	517.33	32.72	1.020	3.65	1.11	2.63	6.13	5436	-0.26	0.111	9.74	0.49	0.053	0.05	0.12	0.65	53.5	0.0444	0.0623
260655847	849.66	49.31	1.020	3.87	0.97	1.91	11.7	5506	-0.01	0	47.41	1.46	0.012	0.18	0.25	1.66	54	0.0192	0
271977529	414.46	25.47	0.989	3.52	1.45	3.47	3.04	4790	0.11	0.02	25.52	2.88	0.055	0.32	0.47	0.26	20.5	0.0061	0.0048
278731442	300.16	20.35	1.001	3.39	1.36	3.91	3.05	4947	-0.3	0	8.52	0.47	0.068	0.16	0.20	0.35	20	0.0124	0
279055252	357.23	24.04	1.009	3.47	1.16	3.3	6.39	5012	0.01	0.026	8.20	2.47	0.065	0.16	0.15	0.69	27	0.0056	0.0053
279090824	553.51	32.49	1.018	3.68	1.38	2.85	2.79	5371	-0.23	0.076	21.12	3.25	0.009	0.06	0.12	0.37	30	0.0093	0.0285
279571746	236.78	16.06	0.994	3.29	1.73	4.99	1.64	4882	0.01	0.021	15.34	0.06	0.009	0.47	0.43	0.16	17.5	0.0067	0.0053
293271686	276.61	18.8	1.005	3.36	1.48	4.23	2.67	5051	0	0	6.44	0.99	0.069	0.10	0.32	0.28	28	0.01	0
300085625	339.99	22.73	0.996	3.44	1.24	3.53	5.49	4811	0.14	0.055	6.24	0.36	0.056	0.14	0.24	0.38	20	0.0059	0.0046
300088321	1173.32	63.28	1.020	4.01	0.97	1.62	11.17	5614	-0.03	0	22.90	1.35	0.038	0.03	0.03	1.74	47.5	0.0312	0

Table 1 *continued*

Table 1 *(continued)*

TIC ID	ν_{max}	$\Delta\nu$	$f_{\Delta\nu}$	$log(g)$	M_{cor}	R_{cor}	Age	T_{eff}	[M/H]	$[\alpha/M]$	$\sigma_{\nu_{max}}$	$\sigma_{\Delta\nu}$	$\sigma_{log(g)}$	$\sigma_{M_{cor}}$	$\sigma_{R_{cor}}$	σ_{Age}	$\sigma_{T_{eff}}$	$\sigma_{[M/H]}$	$\sigma_{\alpha/M}$
	[μHz]	[μHz]	-	[dex]	[$M_\odot$]	[$R_\odot$]	[Gyr]	[K]	-	-	[μHz]	[μHz]	[dex]	[$M_\odot$]	[$R_\odot$]	[Gyr]	[K]	-	-
300161002	403.88	25.5	0.991	3.51	1.34	3.37	3.74	4816	0	0	10.16	0.19	0.044	0.16	0.14	0.40	20	0.01	0
300444376	483.47	27.39	1.010	3.61	1.77	3.48	1.49	5135	-0.03	0.044	38.38	1.42	0.044	0.15	0.19	0.25	33	0.0074	0.0056
349059821	404.48	24.19	1.002	3.52	1.35	3.35	2.97	5017	-0.3	0.179	7.98	1.99	0.030	0.11	0.48	0.35	28	0.0077	0.0696
349374407	224.18	17.03	1.001	3.26	1.13	4.14	5.58	4874	-0.34	0.085	3.86	0.13	0.068	0.19	0.08	0.65	16.5	0.0083	0.0069
349374677	188.96	14.37	0.990	3.18	1.34	4.94	3.16	4757	-0.31	0.065	4.18	0.68	0.057	0.21	0.37	0.35	13.5	0.0079	0.0067
349477633	291.03	19.68	0.999	3.38	1.43	4.07	2.83	4963	-0.11	0.03	2.15	0.58	0.067	0.09	0.13	0.31	17	0.0073	0.0058
349973705	361.63	25.13	1.015	3.48	1.47	3.66	2.7	5219	0	0	11.18	1.45	0.065	0.04	0.14	0.31	47.5	0.01	0
350297922	287.54	20.99	1.013	3.38	1.06	3.5	6.34	5136	-0.45	0.117	2.80	0.52	0.074	0.09	0.10	0.77	37.5	0.0089	0.11
350335258	124.69	10.85	0.998	3.0054	1.46	6.33	2.34	4844	-0.34	0.209	4.42	0.02	0.083	0.04	0.49	0.23	21	0.0067	0.0066
350343922	268.76	19.28	1.008	3.35	1.22	3.89	4.94	5085	-0.17	0.048	5.81	0.20	0.041	0.19	0.16	0.54	29	0.0074	0.0061
350443250	424.08	24.3	1.020	3.56	1.22	3.067	4.23	5263	-0.31	0.069	13.91	1.34	0.021	0.09	0.06	0.47	32	0.0062	0.12
350585437	252.14	18.55	1.009	3.32	1.15	3.92	6.59	5015	0	0	2.05	0.22	0.047	0.16	0.22	0.74	27.5	0.01	0
374858999	456.72	28.04	1.012	3.58	1.37	3.14	3.28	5194	-0.07	0	8.27	0.85	0.049	0.12	0.20	0.37	29	0.0104	0
375089600	354.17	24.85	1.008	3.46	0.98	3.05	11.77	4947	-0.05	0.075	1.28	0.13	0.038	0.12	0.09	1.62	17.5	0.0067	0.0055
381976956	83.52	8.37	1.011	2.84	1.28	7.17	3.16	5022	-0.58	0.103	4.11	0.15	0.074	0.12	0.35	0.33	22.5	0.009	0.0081
382067256	276.55	18.02	0.991	3.35	1.74	4.64	1.67	4842	0.08	0	4.05	0.70	0.025	0.19	0.34	0.26	31.5	0.0125	0
382159212	534.73	30.71	1.014	3.65	1.53	3.07	2.28	5233	0	0	13.39	4.26	0.023	0.27	0.42	0.30	25.5	0.01	0
382302322	403.11	23.87	1.005	3.52	1.13	3.07	5.58	5051	-0.31	0	6.50	1.67	0.063	0.16	0.05	0.66	26	0.0021	0
198383789	325.99	23.33	1.007	3.42	0.96	3.17	11.74	4867	-0.12	0.058	6.89	0.06	0.046	0.14	0.15	1.72	18	0.0071	0.0059
219096868	171.39	13.18	0.994	3.14	1.43	5.34	3.06	4848	-0.02	0.04	4.39	0.19	0.074	0.13	0.47	0.30	16.5	0.0058	0.0053
219792330	441.73	28	1.016	3.56	1.14	2.95	5.92	4954	-0.18	0.102	9.44	0.98	0.033	0.14	0.14	0.72	15	0.0061	0.0946
219801618	263.44	17.6	1.013	3.35	1.68	4.59	1.32	5186	-0.48	0.206	12.27	1.04	0.066	0.18	0.07	0.18	25.5	0.0109	0.19
219856298	385.87	23.19	1.000	3.5	1.15	3.17	5.01	4976	-0.37	0.22	12.27	1.04	0.029	0.15	0.23	0.60	18	0.008	0.0667
224601836	669.31	37.88	1.017	3.76	1.31	2.53	3.69	5308	-0.06	0	40.26	0.54	0.027	0.01	0.04	0.42	28	0.0051	0
224605278	253.3	18.08	0.996	3.31	1.31	4.19	3.99	4876	-0.06	0.053	5.69	0.35	0.068	0.14	0.31	0.38	20	0.0068	0.0056
229606609	171	13.71	0.989	3.14	1.19	4.9	1.28	4707	-0.06	0	2.44	0.60	0.038	0.18	0.32	0.27	18	0.0025	0
229608123	339.24	22.25	1.006	3.45	1.4	3.7	2.77	5076	-0.24	0.082	3.94	1.19	0.061	0.16	0.24	0.31	25.5	0.0062	0.11
229739896	145.78	12.67	0.998	3.069	1.25	5.44	5.05	4753	0.02	0.035	1.47	0.43	0.068	0.18	0.44	0.50	18.5	0.0058	0.0051
229962295	850.85	46.61	1.014	3.88	1.34	2.22	3.48	5766	0.05	-0.019	12.27	1.04	0.027	0.06	0.05	0.43	29.5	0.0103	0.0074
230082687	328.05	21.44	0.996	3.43	1.44	3.86	3.25	4873	0.16	0.033	9.13	0.55	0.067	0.25	0.41	0.24	24	0.0061	0.0048
230088835	316.96	20.21	1.002	3.42	1.67	4.2	1.73	5012	-0.07	0.039	8.86	0.08	0.052	0.20	0.12	0.26	28.5	0.0073	0.0057
230111524	323.08	21.89	1.001	3.42	1.24	3.61	4.42	4878	-0.19	0	2.95	0.14	0.071	0.17	0.05	0.51	29	0.013	0
232610052	245.69	17.9	0.999	3.3	1.22	4.11	4.63	4855	-0.22	0.254	12.27	1.04	0.048	0.15	0.37	0.52	18	0.0071	0.0061
232614734	156.16	11.84	0.993	3.1	1.69	6.06	1.85	4880	0.08	0.007	3.44	0.28	0.065	0.38	0.54	0.14	14.5	0.0063	0.005

Table 1 *continued*

Table 1 *(continued)*

TIC ID	ν_{max}	$\Delta\nu$	$f_{\Delta\nu}$	$log(g)$	M_{cor}	R_{cor}	Age	T_{eff}	[M/H]	$[\alpha/M]$	$\sigma_{\nu_{max}}$	$\sigma_{\Delta\nu}$	$\sigma_{log(g)}$	$\sigma_{M_{cor}}$	$\sigma_{R_{cor}}$	σ_{Age}	$\sigma_{T_{eff}}$	$\sigma_{[M/H]}$	$\sigma_{\alpha/M}$
	[μHz]	[μHz]	-	[dex]	[$M_\odot$]	[$R_\odot$]	[Gyr]	[K]	-	-	[μHz]	[μHz]	[dex]	[$M_\odot$]	[$R_\odot$]	[Gyr]	[K]	-	-
233047757	199.57	16.71	1.004	3.2	1.21	4.57	5.96	4736	0.11	0.084	3.27	0.49	0.059	0.16	0.30	0.41	17.5	0.0057	0.0047
233050540	340.57	22.15	1.008	3.45	1.44	3.75	2.36	5120	-0.33	0.084	12.27	1.04	0.062	0.15	0.20	0.29	24	0.0064	0.11
233053435	211.72	15.84	0.998	3.24	1.27	4.53	4.66	4840	0	0	5.22	0.12	0.070	0.20	0.12	0.48	29.5	0.01	0
233056745	597.55	35.68	1.005	3.69	1.11	2.51	7.18	4947	-0.02	0.043	25.64	2.13	0.039	0.11	0.12	0.74	23.5	0.0057	0.0535
233678984	442.09	31.69	1.016	3.57	1.26	3.07	3.73	5214	-0.32	0.084	12.27	1.04	0.026	0.12	0.08	0.44	26.5	0.009	0.0452
233680706	246.62	18.73	1.007	3.31	1.019	3.74	9.58	4928	-0.1	0	12.27	1.04	0.062	0.06	0.09	1.16	22.5	0.0003	0
233683095	245.19	18.84	1.005	3.3	0.98	3.68	10.99	4896	-0.11	0.072	3.71	0.17	0.046	0.13	0.06	1.47	16.5	0.0069	0.0058
258389994	212.84	16.07	1.000	3.24	1.24	4.45	4.52	4930	-0.18	0.079	1.34	0.04	0.042	0.20	0.27	0.51	20	0.0074	0.0061
264222470	353.42	22.42	1.002	3.46	1.52	3.81	2.38	5001	-0.02	0.035	6.34	1.06	0.062	0.17	0.23	0.26	24.5	0.007	0.0067
272784360	269.93	19.9	1.010	3.35	1.07	3.65	6.63	5043	-0.36	0	3.66	0.07	0.058	0.07	0.06	0.81	26.5	0.019	0
287140025	301.89	20.8	1.005	3.4	1.27	3.76	4.29	5005	-0.11	0	2.28	1.04	0.036	0.17	0.33	0.48	18.5	0.0005	0
307985358	158.38	12.5	0.989	3.11	1.4	5.5	3.56	4782	0.1	0.026	1.52	0.43	0.074	0.09	0.47	0.25	18	0.0064	0.0055
332503809	359.41	25.68	1.008	3.47	0.88	2.88	14.47	4899	-0.26	0.176	16.36	1.23	0.047	0.14	0.17	1.98	11	0.0074	0.0708
356111938	415.91	26.71	1.001	3.53	1.19	3.12	6.37	4866	0.15	0.041	9.25	1.02	0.060	0.15	0.04	0.40	19.5	0.0061	0.0048
360019958	209.34	15.4	0.977	3.22	1.37	4.8	3.67	4563	0.04	0.021	7.55	0.07	0.036	0.17	0.19	0.35	21	0.0063	0.0051
366490487	140.89	13.23	1.018	3.09	0.86	4.42	21.16	5499	0.18	-0.031	12.27	1.04	0.796	0.32	2.36	3.35	22.5	0.007	0.005
441731916	405.29	27.53	1.008	3.52	0.95	2.83	13.21	4882	0.01	0.137	12.27	1.04	0.037	0.13	0.11	1.89	15.5	0.0064	0.0142

NOTE—The data table for the entire sample. The listed ν_{max}, $\Delta\nu$, $log(g)$, M_{cor}, and R_{cor} are our calculated seismic values. The ν_{max}, $\Delta\nu$, and $log(g)$ uncertainties are found from taking the difference between our sample and previous literature and subtracting the previous literature's uncertainties in quadrature. The M_{cor} and R_{cor} uncertainties are found by propagating forward the uncertainties on the ν_{max}, $\Delta\nu$, T_{eff}, $f_{\nu_{max}}$, and $f_{\Delta\nu}$. The listed T_{eff}, [M/H], and [α/M] values are spectroscopic with T_{eff} and [M/H] calibrated in Godoy-Rivera et al. (2021) and [α/M] directly from APOGEE DR16. The T_{eff} and [M/H] uncertainties are taken directly from Godoy-Rivera et al. (2021) and the [α/M] uncertainties are taken directly from APOGEE DR16. The listed $f_{\Delta\nu}$ values are given by ASFGrid (Sharma & Stello 2016). The average $f_{\nu_{max}}$ value is 0.9877 and is found by calibrating our computed luminosity to the *Gaia* luminosity calibrated in Godoy-Rivera et al. (2021). The listed age is the average age from the YREC, MIST, DSEP, and GARSTEC model grids. The age uncertainties are the average observational and theoretical errors from the four stellar model grids added in quadrature. The separate average observational and average theoretical age uncertainties are listed in Table 2.

Table 2. Age Values and Uncertainties

TIC ID	YREC Ages	MIST Ages	DSEP Ages	GARSTEC Ages	$\sigma_{Age_{the}}$	$\sigma_{Age_{obs}}$
25156036	8.01	7.81	7.64	7.75	0.16	0.39
31506424	5.47	4.98	5.37	5.35	0.22	0.45
38602419	8.18	7.14	7.78	7.93	0.44	0.84
41587424	3	2.7	2.99	2.97	0.14	0.24
55270123	7.33	6.57	7.15	7.17	0.33	0.63
141335100	6.38	6.31	5.84	6.29	0.25	0.1
141626634	2.06	1.87	2.09	1.93	0.1	0.1
141757732	2.23	2.01	2.22	2.21	0.1	0.18
142109390	2.62	2.43	2.66	2.58	0.1	0.21
149390710	8.49	7.32	8.08	8.26	0.5	0.87
150030411	7.09	6.94	6.7	6.86	0.16	0.28
150062447	8.67	7.66	8.32	8.42	0.43	2.96
150166759	6.92	6.51	6.64	6.75	0.17	0.46
150393198	7.85	7.09	7.72	7.73	0.34	0.68
150430044	3.5	3.39	3.5	3.41	0.06	0.13
150442152	2.96	2.78	3.01	2.94	0.1	0.13
167342488	3.03	2.71	3.02	3	0.15	0.27
167548586	2.96	2.73	3.01	2.93	0.12	0.23
177241155	4.52	3.98	4.32	4.45	0.24	0.4
220457103	3.9	3.45	3.71	3.79	0.19	0.35
257720189	8.01	7.44	7.73	7.85	0.24	0.61
260078030	6.56	5.81	6.41	6.42	0.33	0.56
260655847	12.81	11.27	12.06	12.18	0.63	1.54
271977529	3.38	3.18	3.4	3.34	0.1	0.24
278731442	3.4	3.02	3.33	3.37	0.18	0.3
279055252	6.89	6.25	6.61	6.74	0.27	0.63
279090824	3.13	2.73	3.13	3.01	0.19	0.32
279571746	1.72	1.58	1.74	1.65	0.07	0.14
293271686	2.91	2.62	2.98	2.86	0.15	0.24
300085625	5.97	5.68	5.75	5.84	0.13	0.36
300088321	12.47	10.91	11.61	11.74	0.64	1.62
300161002	4.27	3.9	4.19	4.24	0.17	0.36
300444376	5.29	4.81	5.07	5.19	0.21	0.13
349059821	3.4	3.02	3.33	3.38	0.18	0.3
349374407	6.27	5.54	6.07	6.16	0.32	0.57
349374677	3.57	3.17	3.47	3.56	0.18	0.3
349477633	3.16	2.83	3.14	3.13	0.16	0.27
349973705	2.91	2.62	2.99	2.77	0.16	0.27
350297922	6.95	6.2	6.64	6.79	0.32	0.7
350335258	2.59	2.33	2.57	2.57	0.12	0.2
350343922	5.11	4.51	4.88	5	0.26	0.47
350443250	4.62	4.1	4.46	4.51	0.23	0.41
350585437	7.03	6.34	6.74	6.88	0.3	0.68
374858999	3.62	3.25	3.61	3.53	0.17	0.33
375089600	12.77	11.22	12.14	12.27	0.65	1.48

Table 2 *continued*

Table 2 *(continued)*

TIC ID	YREC Ages	MIST Ages	DSEP Ages	GARSTEC Ages	$\sigma_{Age_{the}}$	$\sigma_{Age_{obs}}$
381976956	3.45	3.13	3.32	3.38	0.14	0.3
382067256	7.29	6.75	7.01	7.13	0.23	0.12
382159212	2.58	2.33	2.64	2.43	0.14	0.26
382302322	6.16	5.4	6.01	6.06	0.34	0.56
198383789	13.32	11.52	12.67	12.84	0.76	1.54
219096868	3.35	3.05	3.34	3.33	0.14	0.27
219792330	6.69	5.87	6.5	6.58	0.37	0.62
219801618	2.91	2.62	2.83	2.85	0.13	0.13
219856298	5.63	4.98	5.41	5.52	0.29	0.52
224601836	4.11	3.76	4.01	4.04	0.15	0.39
224605278	4.43	4.04	4.3	4.4	0.18	0.33
229606609	6.39	5.79	6.18	6.24	0.25	0.1
229608123	3.12	2.74	3.1	3.08	0.18	0.25
229739896	5.54	5.08	5.27	5.45	0.2	0.46
229962295	3.95	3.63	3.95	3.8	0.15	0.4
230082687	3.56	3.38	3.59	3.51	0.09	0.22
230088835	4	3.56	3.88	3.96	0.2	0.17
230111524	5	4.43	4.77	4.92	0.26	0.44
232610052	5.2	4.6	5	5.1	0.27	0.44
232614734	1.52	1.44	1.55	1.44	0.05	0.13
233047757	6.47	6.17	6.27	6.31	0.12	0.39
233050540	2.64	2.32	2.61	2.59	0.15	0.25
233053435	5.1	4.64	4.87	5.04	0.21	0.43
233056745	7.89	7.14	7.69	7.79	0.33	0.66
233678984	4.12	3.61	3.9	4	0.22	0.38
233680706	10.58	9.34	10.19	10.32	0.54	1.027
233683095	12.47	10.88	11.91	12.06	0.68	1.3
258389994	4.96	4.39	4.72	4.88	0.25	0.44
264222470	2.63	2.38	2.68	2.6	0.13	0.23
272784360	7.26	6.4	7.02	7.11	0.38	0.71
287140025	4.75	4.22	4.5	4.68	0.24	0.41
307985358	3.87	3.67	3.88	3.82	0.1	0.23
332503809	6.03	5.26	5.8	5.91	0.34	1.95
356111938	6.86	6.54	6.55	6.69	0.15	0.37
360019958	4.11	3.83	4.08	4.26	0.18	0.3
366490487	16.99	13.06	12.53	13.56	2.01	2.68
441731916	14.77	12.98	13.83	14.16	0.75	1.74

NOTE—The ages for the YREC, MIST, DSEP, and GARSTEC stellar model grids for the entire sample. The Age_{the} error is the average theoretical error given by `Kiauhoku` between the 4 model grids. The Age_{obs} error is the average observational error calculated by propagating forward the uncertainty on the mass and metallicity. The units for all ages and the error is in Gyr.